On a hemi-variational formulation for a 2D elasto-plastic-damage strain gradient solid with granular microstructure

Luca Placidi, Emilio Barchiesi, Francesco Dell'Isola, Valerii Maksimov, Anil Misra, Nasrin Rezaei, Angelo Scrofani, Dmitry Timofeev

Research article

On a hemi-variational formulation for a 2D elasto-plastic-damage strain gradient solid with granular microstructure†

Luca Placidi[1,*], Emilio Barchiesi[2,3,5], Francesco dell'Isola[2], Valerii Maksimov[1], Anil Misra[4], Nasrin Rezaei[1], Angelo Scrofani[2] and Dmitry Timofeev[2]

[1] Faculty of Engineering, International Telematic University UNINETTUNO, Rome, Italy

[2] International Research Center on Mathematics and Mechanics of Complex Systems (M&MoCS), Università degli Studi dell'Aquila, L'Aquila, Italy

[3] École Nationale d'Ingénieurs de Brest, 760 ENIB, UMR CNRS 6027, IRDL, F-29200 Brest, France

[4] Civil, Environmental and Architectural Engineering Department, The University of Kansas, Kansas City, Kansas, USA

[5] Université de Bretagne Sud, Rue de Saint Maudé - BP 92116 56321, Lorient, Cedex, France

* **Correspondence:** Email: luca.placidi@uninettunouniversity.net; Tel: 066920761 Ext. 217.

Abstract: We report a continuum theory for 2D strain gradient materials accounting for a class of dissipation phenomena. The continuum description is constructed by means of a (reversible) placement function and by (irreversible) damage and plastic functions. Besides, expressions of elastic and dissipation energies have been assumed as well as the postulation of a hemi-variational principle. No flow rules have been assumed and plastic deformation is also compatible , that means it can be derived by a placement function. Strain gradient Partial Differential Equations (PDEs), boundary conditions (BCs) and Karush-Kuhn-Tucker (KKT) type conditions are derived by a hemi variational principle. PDEs and BCs govern the evolution of the placement descriptor and KKT conditions that of damage and plastic variables. Numerical experiments for the investigated homogeneous cases do not need the use of Finite Element simulations and have been performed to show the applicability of the model. In particular, the induced anisotropy of the response has been investigated and the coupling between damage and plasticity evolution has been shown.

Keywords: damage mechanics; granular microstructures; Karush-Kuhn-Tucker conditions; strain gradient; 2D continua

1. Introduction

A large amount of scientific literature deals with non-conservative physical systems, where it is necessary to use methods that are able to handle the related dissipation phenomena [3, 16, 28, 38, 54]. In engineering applications [39, 40, 62] a wide range of materials, like steel and concrete, experience dissipative phenomena such as damage and plasticity. That is why they are especially interesting for the engineering community. But building accurate description of these phenomena can be very difficult, especially for complex material systems like granular [39] or lattice-type [25, 58] microstructure. Continuum damage [1, 8] and plasticity [4, 9, 17, 22–24, 32, 39, 40, 49, 50] modeling have been vigorously pursued in the literature, considering the improvements based on phase field models [10, 13, 14, 33, 35, 55] for shear bands and fracture. Multi-scale approaches [6, 27, 34, 42] , in addition to phenomenological ones [56, 57], have been proposed. Their purpose is to link low-scale descriptions with continuum [15, 29, 31] to include complex emerging behaviors in the continuum. Besides, the strain gradient regularization of the elastic response [26, 30] should be considered also in this non conservative context. In this paper we recap, in a new and better way, recently developed continuum model for granular materials undergoing damage and plastic deformations. Damage and plasticity are irreversible phenomena [2, 32, 49, 50]. In this model, the irreversibility is taken into account by assuming that damage and plastic variables are non-decreasing quantities in time [59]. It has been extensively discussed in the literature, that deformed shapes of granular materials may be described in a continuum model by using the relative displacements of the barycenters of the grains, regardless their deformations. Thus, in a coarse-grained description, for a material with a granular micro-structure, the deformation energy as well as the energy dissipated due to damage and plasticity, are expressed in terms of these relative movements. The volumetric energy of deformation, i.e., the deformation energy per unit volume, is assumed to be the sum of deformation energies associated with each intergranular interaction. Each grain-grain interaction is identified by the orientation of the grain-grain direction that, in the continuum limit, are infinite in number. This approach has shown its efficiency in describing granular systems, both at the discrete and at the continuum levels [5, 7, 18, 37, 51, 60, 61]. We also use a variational approach [20, 21]. First of all, we define an objective and reversible kinematic vector variable to measure the relative displacements between grains. Thus, we decompose the objective relative displacement between the grains [39, 48] into two components. The first one is directed along the vector connecting the grain centroids, and it is called the normal component. The second is directed along the orthogonal direction and is called the tangent component. These components are decomposed into elastic and plastic parts. The functionals of elastic deformation and of dissipation energy are defined in terms of these reversible components [52, 53] and of irreversible damage and plastic variables. Damage is defined by two variables, i.e., the normal and the tangential damage variables, that are both a function of grain-grain orientation. On the one part, plastic displacement does not have to be non-decreasing in time. On the other part, it is characterized as the difference between two non-diminishing plastic variables, that are the accumulated plastic relative displacement in tension and in compression, respectively. The evolution of the form of the body that is obtained without external load defines in this approach the evolution of the plastic strain. The elastic evolution of the damaged material is defined by the total elastic strain energy. This type of energy is explained in terms of the elastic energies related to each intergranular orientation. Therefore, dependencies are obtained for the standard elastic modules (4th

order stiffness tensor), of the second gradient elastic modules (6th order stiffness tensor) and of the chiral interaction modules (5th order stiffness tensor). They are functions of parameters describing the damage-elasto-plastic state, describing micro-mechano-morphology, of each orientation. Besides, because of plastic effects, we obtain an expression also of the pre-stress (2nd order tensor) and of the pre-hyperstress (3rd order tensor). The hemi-variational approach [43–46] has been used to obtain Karush-Kuhn-Tucker (KKT) kind conditions, that drive the evolution of damage and plastic irreversible kinematic variables. According to the same derivation, also the Euler-Lagrange equations for the progress of the reversible placement function is obtained. It is worth to be noted that, since grain-pairs are oriented in different directions, for a given loading-sequence, they experience different loads and hence different damage and plastic evolution. Thus, the macroscopic response will be complex and with an intrinsically dependence upon path.

The content of this paper is organized as follows. Section 2 provides a rational recap of the model that was introduced in papers [12,41,44,47,59]. Section 3 provides the scheme of a possible numerical (or analytical) implementation of the model. Section 4 is devoted to the representation of the results for the homogeneous case, where no Finite Element implementation is necessary for the illustration of the results. Section 5 addresses a few concluding comments and future viewpoints.

2. A rational recap of the model

In this section we will recap the model that has been investigated by the authors more widely in different papers [12, 41, 44, 47, 59].

2.1. The elastic energy per unit area

Let $\mathcal{B}$ be the $2D$ reference configuration of a strain gradient elastic body. Its elastic energy U per unit area is assumed to take the following form

$$U = \int_{\mathcal{S}^1} \left[\frac{1}{2} k_{\eta,D} \left(u_\eta^{el} \right)^2 + \frac{1}{2} k_{\tau,D} \left(u_\tau^2 \right) \right], \qquad \forall \boldsymbol{X} \in \mathcal{B} \tag{2.1}$$

where the elastic part u_η^{el} of the normal displacement u_η is postulated be equal to the difference of the total normal displacement u_η and its plastic part u_η^{pl}

$$u_\eta^{el} = u_\eta - u_\eta^{pl}, \tag{2.2}$$

where u_τ is the tangential displacement and both are defined as follows,

$$u_\eta = L G_{ij} \hat{c}_i \hat{c}_j + \frac{L^2}{4} G_{ij,h} \hat{c}_i \hat{c}_j \hat{c}_h, \tag{2.3}$$

$$u_\tau^2 = 4L^2 G_{ij} G_{ab} \left(\delta_{ia} \hat{c}_j \hat{c}_b - \hat{c}_i \hat{c}_j \hat{c}_a \hat{c}_b \right) + 2L^3 G_{ij} G_{ab,c} \left(\delta_{ia} \hat{c}_j \hat{c}_b \hat{c}_c - \hat{c}_i \hat{c}_j \hat{c}_a \hat{c}_b \hat{c}_c \right) \tag{2.4}$$

$$+ \frac{L^4}{4} G_{ij,h} G_{am,n} \left(\delta_{ia} \hat{c}_j \hat{c}_h \hat{c}_m \hat{c}_n - \hat{c}_i \hat{c}_j \hat{c}_h \hat{c}_a \hat{c}_b \hat{c}_c \right),$$

where the unit vector $\hat{c}$ gives the direction of the considered grain-pair interaction and the domain $\mathcal{S}^1$ is the unit circle to which it belongs; the Green-Saint-Venant tensor G and its gradient are tensors of a 2nd and 3rd order,

$$G = \frac{1}{2} \left(F^T F - I \right), \quad \nabla G = F^T \nabla F, \tag{2.5}$$

respectively, where the deformation gradient F and its gradient are defined

$$F = \nabla\boldsymbol{\chi}, \qquad \nabla F = \nabla\left(\nabla\boldsymbol{\chi}\right) \tag{2.6}$$

in terms of the placement function $\boldsymbol{\chi}\left(\boldsymbol{X}, t\right)$, that is a function of the position X and of time t. In Eq (2.3) and (2.4), L is the averaged grain-pair distance. Besides, the damaged tangent stiffness is $k_{\tau,D}$ and the damaged normal stiffness is $k_{\eta,D}$. The damaged normal stiffness is assumed to be asymmetric in tension and compression, i.e.,

$$k_{\eta,D} = k^t_{\eta,D}\Theta\left(u^{el}_\eta\right) + k^c_{\eta,D}\Theta\left(-u^{el}_\eta\right), \tag{2.7}$$

where $k^t_{\eta,D}$ is the stiffness in tension that is assumed to be smaller than the stiffness in compression $k^c_{\eta,D} \gg k^t_{\eta,D}$. Besides, the dividing line between tension and compression is given by the sign of the elastic normal displacement u^{el}_η. Thus, the Heaviside function Θ is here used. Damage is modeled, as we have already pointed out, with two variables, i.e., the normal damage D_η, and the tangent damage D_τ. The damage variables D_η and D_τ have the role to reduce the damaged normal stiffness $k_{\eta,D}$ (2.7) and the damaged tangent stiffness $k_{\tau,D}$, respectively,

$$k_{\eta,D} = k_\eta\left(1 - D_\eta\right), \qquad k_{\tau,D} = k_\tau\left(1 - D_\tau\right), \tag{2.8}$$

where the non-damaged normal stiffness k_η and the non-damaged tangent stiffness k_τ have been introduced. Definitions of non-damaged tension (k^t_η) and compression (k^c_η) normal stiffness through the following expressions

$$k^t_{\eta,D} = k^t_\eta\left(1 - D_\eta\right), \qquad k^c_{\eta,D} = k^c_\eta\left(1 - D_\eta\right), \tag{2.9}$$

yield the analogous of (2.7) for the non-damaged normal stiffness, i.e.,

$$k_\eta = k^t_\eta\Theta\left(u^{el}_\eta\right) + k^c_\eta\Theta\left(-u^{el}_\eta\right). \tag{2.10}$$

We therefore obtain, by insertion of (2.10) into $(2.8)_1$, the following expression for the damaged normal stiffness

$$k_{\eta,D} = k_\eta\left(1 - D_\eta\right) = k^t_\eta\left(1 - D_\eta\right)\Theta\left(u^{el}_\eta\right) + k^c_\eta\left(1 - D_\eta\right)\Theta\left(-u^{el}_\eta\right). \tag{2.11}$$

Insertion of (2.2), (2.3), (2.4) and (2.8) into (2.1) yield the elastic energy per unit area in a more compact form as

$$U = \frac{1}{2}\mathbb{C}_{ijab}G_{ij}G_{ab} + \mathbb{M}_{ijabc}G_{ij}G_{ab,c} + \frac{1}{2}\mathbb{D}_{ijhabc}G_{ij,h}G_{ab,c} + \mathbb{P}_{ij}G_{ij} + \mathbb{Q}_{ijh}G_{ij,h}, \tag{2.12}$$

where, accounting for the symmetrization induced by the symmetry of the strain tensor G, the elastic stiffnesses $\mathbb{C}$, $\mathbb{M}$, $\mathbb{D}$, $\mathbb{P}$ and $\mathbb{Q}$ are identified as follows

$$\begin{aligned}\mathbb{C}_{ijab} &= L^2\int_{\mathcal{S}^1} k_\eta\left(1 - D_\eta\right)\hat{c}_i\hat{c}_j\hat{c}_a\hat{c}_b \\ &+L^2\int_{\mathcal{S}^1} k_\tau\left(1 - D_\tau\right)\left(\left(\delta_{ia}\hat{c}_j\hat{c}_b + \delta_{ib}\hat{c}_j\hat{c}_a + \delta_{ja}\hat{c}_i\hat{c}_b + \delta_{jb}\hat{c}_i\hat{c}_a\right) - 4\hat{c}_i\hat{c}_j\hat{c}_a\hat{c}_b\right)\end{aligned} \tag{2.13}$$

$$\mathbb{M}_{ijabc} = \frac{1}{4}L^3 \int_{\mathcal{S}^1} k_\eta \left(1 - D_\eta\right) \hat{c}_i \hat{c}_j \hat{c}_a \hat{c}_b \hat{c}_c \tag{2.14}$$
$$+\frac{1}{4}L^3 \int_{\mathcal{S}^1} k_\tau \left(1 - D_\tau\right) \left(\left(\delta_{ia}\hat{c}_j\hat{c}_b + \delta_{ib}\hat{c}_j\hat{c}_a + \delta_{ja}\hat{c}_i\hat{c}_b + \delta_{jb}\hat{c}_i\hat{c}_a\right)\hat{c}_c - 4\hat{c}_i\hat{c}_j\hat{c}_a\hat{c}_b\hat{c}_c\right)$$
$$\mathbb{D}_{ijhabc} = \frac{1}{16}L^4 \int_{\mathcal{S}^1} k_\eta \left(1 - D_\eta\right) \hat{c}_i \hat{c}_j \hat{c}_h \hat{c}_a \hat{c}_b \hat{c}_c \tag{2.15}$$
$$+\frac{1}{16}L^4 \int_{\mathcal{S}^1} k_\tau \left(1 - D_\tau\right) \left(\left(\delta_{ia}\hat{c}_j\hat{c}_b + \delta_{ib}\hat{c}_j\hat{c}_a + \delta_{ja}\hat{c}_i\hat{c}_b + \delta_{jb}\hat{c}_i\hat{c}_a\right)\hat{c}_h\hat{c}_c - 4\hat{c}_i\hat{c}_j\hat{c}_h\hat{c}_a\hat{c}_b\hat{c}_c\right)$$
$$\mathbb{P}_{ij} = -L \int_{\mathcal{S}^1} k_\eta \left(1 - D_\eta\right) u_\eta^{pl} \hat{c}_i \hat{c}_j \tag{2.16}$$
$$\mathbb{Q}_{ijh} = -\frac{1}{4}L^2 \int_{\mathcal{S}^1} k_\eta \left(1 - D_\eta\right) u_\eta^{pl} \hat{c}_i \hat{c}_j \hat{c}_h \tag{2.17}$$

According to the legacy of strain gradient continua [11, 19], a consequence of the expression (2.12) for the elastic energy per unit area is the form of both the stress tensor S and the hyper stress tensor T, i.e.,

$$S_{ij} = \frac{\partial U}{\partial G_{ij}} = \mathbb{P}_{ij} + \mathbb{C}_{ijab}G_{ab} + \mathbb{M}_{ijabc}G_{ab,c}, \qquad T_{ijh} = \frac{\partial U}{\partial G_{ij,h}} = \mathbb{Q}_{ijh} + \mathbb{D}_{ijhabc}G_{ab,c} + \mathbb{M}_{ijhab}G_{ab}, \tag{2.18}$$

where $\mathbb{P}$ and $\mathbb{Q}$ take the roles of the pre-stress and the pre-hyper stress, respectively. We oversee that (i) the normal plastic displacement u_η^{pl} has a direct influence, as expected, from (2.16)–(2.17) on the pre-stress and on the pre-hyper stress and (ii) damage variables D_η and D_τ has a direct influence from (2.13)–(2.17) on all the stiffness tensors.

2.2. The dissipation energy per unit area

Damage and plastic variables are dissipative in nature and their evolution are related to the form of the dissipation energy. The dissipation energy per unit area W is the energy dissipated because of irreversible phenomena. An additive decomposition of the dissipation energy is assumed in terms of $W_D = W_D^\eta + W_D^\tau$, the energy dissipated because of damage phenomena (where W_D^η is the part that is due to the normal phenomena and W_D^τ is the part that is due to tangential phenomena), and W_{pl}, the energy dissipated because of plasticity phenomena, i.e.,

$$W = W_D + W_{pl} = W_D^\eta + W_D^\tau + W_{pl}, \tag{2.19}$$
$$W_D^\eta = \int_{\mathcal{S}^1} \frac{1}{2}k_\eta^c \left(B_\eta^c\right)^2 \Theta\left(-u_\eta^{el}\right)\left[-D_\eta + \frac{2}{\pi}\tan\left(\frac{\pi}{2}D_\eta\right)\right] \tag{2.20}$$
$$+ \int_{\mathcal{S}^1} \frac{1}{2}k_\eta^t \left(B_\eta^t\right)^2 \Theta\left(u_\eta^{el}\right)\left[2 + \left(D_\eta - 1\right)\left(2 - 2\log\left(1 - D_\eta\right) + \left(\log\left(1 - D_\eta\right)\right)^2\right)\right],$$
$$W_D^\tau = \int_{\mathcal{S}^1} \frac{1}{2}k_\tau \left[\widetilde{B}_\tau\left(u_\eta^{el}\right)\right]^2 \left[2 + \left(D_\tau - 1\right)\left(2 - 2\log\left(1 - D_\tau\right) + \left(\log\left(1 - D_\tau\right)\right)^2\right)\right], \tag{2.21}$$
$$W_{pl} = \int_{\mathcal{S}^1} \sigma_\eta^t \lambda_\eta^t + \sigma_\eta^c \lambda_\eta^c, \tag{2.22}$$

where B_η^c and B_η^t are two characteristic displacements associated with normal damage dissipation in compression and in tension, respectively. The complicated forms of the assumed dissipated energy

in (2.20)–(2.21) are devoted to obtain, in the subsection 2.5, an exponential and/or an arctangential damage evolution, as it will be proved in (2.42) and (2.43).

For cementitious materials it is intuitive that $B_\eta^t \ll B_\eta^c$. The reason is that, in tension, a smaller amount of elastic normal displacement is needed to activate damage mechanisms. Besides, $\widetilde{B}_\tau\left(u_\eta^{el}\right)$ is the characteristic displacement associated with tangent damage dissipation. It is assumed to depend on u_η^{el}, i.e., on the elastic part of the normal displacement as follows,

$$B_\tau = \widetilde{B}_\tau\left(u_\eta^{el}\right) = \begin{cases} B_{\tau 0} & \text{if } u_\eta^{el} \geq 0 \\ B_{\tau 0} - \alpha_2 u_\eta^{el} & \text{if } \frac{1-\alpha_1}{\alpha_2} B_{\tau 0} \leq u_\eta^{el} < 0 \\ \alpha_1 B_{\tau 0} & \text{if } u_\eta^{el} < B_{\tau 0}\frac{1-\alpha_1}{\alpha_2}, \end{cases} \tag{2.23}$$

where $B_{\tau 0}$, α_1 and α_2 are necessary constitutive parameters needed to express the function $\widetilde{B}_\tau\left(u_\eta^{el}\right)$. These parameters have the role to couple the two terms, namely the addends (2.20) and (2.21), of the damage dissipation energy W_D per unit area. It is worth to be noted that usually, for cementitious materials and in elastic tension, the characteristic tangential displacement $B_\tau = B_{\tau 0}$ is much lower than the one $B_\tau = \alpha_1 B_{\tau 0}$ it is necessary in elastic compression ($\alpha_1 \gg 1$). Indeed, a smaller amount of elastic tangential displacement is needed in elastic extension to activate tangential damage mechanisms with respect to the tangential displacement that is needed in elastic compression. In other words, referring to Eq (2.23), this means both that $B_{\tau 0} < B_{\tau 0} - \alpha_2 u_\eta^{el}$ (which implies $\alpha_2 > 0$, as $u_\eta^{el} < 0$ in compression) and $B_{\tau 0} << \alpha_1 B_{\tau 0}$ (which implies $\alpha_1 \gg 1$).

The plastic dissipation energy function per unit area W_{pl} in (2.22) is assumed to linearly depend on the plastic multipliers λ_η^t and λ_η^c that are the plastic accumulated displacement in tension and in compression, respectively. The plastic normal displacement is defined as the following difference,

$$u_\eta^{pl} = \lambda_\eta^t - \lambda_\eta^c. \tag{2.24}$$

We will show at the end of Subsection 2.5 that the scalars σ_η^t and σ_η^c, defined in (2.22), dictate the yielding conditions (more specifically, they are the characteristic force that is necessary to apply to the grain-pair to activate plastic deformation for no-damage case) of the damage-elasto-plastic grain-pair interaction in tension and compression, respectively. It is worth to be noted that the identification of newly introduced constitutive parameters, i.e. of L, B_η^t, B_η^c, $B_{\tau 0}$, α_1 and α_2, is necessary for the application of the present approach for modeling the mechanical behavior or real materials such as, e.g., concrete.

2.3. The energy functional

The energy functional is defined as the sum of the elastic and dissipation energy,

$$\mathcal{E}\left(\chi, D_\eta, D_\tau, \lambda_\eta^t, \lambda_\eta^c\right) = \int_{\mathcal{B}} U + W, \tag{2.25}$$

integrated over the $2D$ reference configuration $\mathcal{B}$. It is a functional of the fundamental kinematical descriptors of the model, i.e. the placement

$$\chi\left(\boldsymbol{X}, t\right), \tag{2.26}$$

that is a function of position $\boldsymbol{X}$ and time t, and the 4 irreversible descriptors

$$D_\eta\left(\boldsymbol{X},\hat{c},t\right), D_\tau\left(\boldsymbol{X},\hat{c},t\right), \lambda_\eta^t\left(\boldsymbol{X},\hat{c},t\right), \lambda_\eta^c\left(\boldsymbol{X},\hat{c},t\right), \tag{2.27}$$

that are functions not only of position X and time t but also on the orientation $\hat{c}$.

Damage (D_η and D_τ) and plastic (λ_η^t and λ_η^c) variables are defined both by two variables that are non-decreasing in time. These inequality assumptions,

$$\frac{\partial D_\eta}{\partial t} \geq 0, \quad \frac{\partial D_\tau}{\partial t} \geq 0, \quad \frac{\partial \lambda_\eta^t}{\partial t} \geq 0, \quad \frac{\partial \lambda_\eta^c}{\partial t} \geq 0, \quad \forall \boldsymbol{X} \in \mathcal{B}, \quad \forall \hat{c} \in \mathcal{S}^1, \tag{2.28}$$

imply a generalization of standard variational principle into a so-called hemivariational principle.

2.4. The hemivariational inequality principle

Let us introduce a monotonously increasing time sequence $T_i \in \{T_i\}_{i=0,\ldots,M}$ with $T_i \in \mathbb{R}$ and $M \in \mathbb{N}$ and give initial datum on each of the fundamental kinematic quantities for $i = 0$, i.e., for time T_0. A family of placements χ defines the motion for each time $t = T_0, T_1, \ldots, T_M$. The set AM_t of kinematically admissible placements is defined for a given time t and the set AV_t is defined as the corresponding space of kinematically admissible variations, i.e., $\upsilon = \delta\chi \in AV_t$. Admissible variations β of the irreversible kinematic quantities $\left(D_\eta, D_\tau, \lambda_\eta^t, \lambda_\eta^c\right)$ must be positive, namely

$$\beta = \delta D_\eta, \delta D_\tau, \delta\lambda_\eta^t, \delta\lambda_\eta^c \in \mathbb{R}^+ \times \mathbb{R}^+ \times \mathbb{R}^+ \times \mathbb{R}^+. \tag{2.29}$$

By definition, the first variation $\delta\mathcal{E}$ of the energy functional (2.25) is calculated as

$$\delta\mathcal{E} = \mathcal{E}\left(\chi + \delta\chi, D_\eta + \delta D_\eta, D_\tau + \delta D_\tau, \lambda_\eta^t + \delta\lambda_\eta^t, \lambda_\eta^c + \delta\lambda_\eta^c\right) - \mathcal{E}\left(\chi, D_\eta, D_\tau, \lambda_\eta^t, \lambda_\eta^c\right). \tag{2.30}$$

Besides, the increment of (2.26-2.27), i.e. of the fundamental kinematic quantities, at $t = T_i$ is given by the difference between these quantities as evaluated at times $t = T_i$ and $t = T_{i-1}$, namely

$$\left(\Delta\chi, \Delta D_\eta, \Delta D_\tau, \Delta\lambda_\eta^t, \Delta\lambda_\eta^c\right)_{T_i} = \left(\chi, D_\eta, D_\tau, \lambda_\eta^t, \lambda_\eta^c\right)_{T_i} - \left(\chi, D_\eta, D_\tau, \lambda_\eta^t, \lambda_\eta^c\right)_{T_{i-1}}. \tag{2.31}$$

The same definition is utilized for the increment $\Delta\mathcal{E}$ of the energy functional

$$\Delta\mathcal{E} = \mathcal{E}\left(\chi + \Delta\chi, D_\eta + \Delta D_\eta, D_\tau + \Delta D_\tau, \lambda_\eta^t + \Delta\lambda_\eta^t, \lambda_\eta^c + \Delta\lambda_\eta^c\right) - \mathcal{E}\left(\chi, D_\eta, D_\tau, \lambda_\eta^t, \lambda_\eta^c\right). \tag{2.32}$$

Finally, as a matter of facts, the hemi-variational principle is formulated as follows

$$\Delta\mathcal{E} \leq \delta\mathcal{E} \qquad \forall\upsilon = \delta\chi \in AV_t, \qquad \forall\beta = \left(\delta D_\eta, \delta D_\tau, \delta\lambda_\eta^t, \delta\lambda_\eta^c\right) \in \mathbb{R}^+ \times \mathbb{R}^+ \times \mathbb{R}^+ \times \mathbb{R}^+. \tag{2.33}$$

It is worth to be noted here that introducing the three vectors

$$A = \left(\frac{\partial\mathcal{E}}{\partial\chi}, \frac{\partial\mathcal{E}}{\partial D_\eta}, \frac{\partial\mathcal{E}}{\partial D_\tau}, \frac{\partial\mathcal{E}}{\partial\lambda_\eta^t}, \frac{\partial\mathcal{E}}{\partial\lambda_\eta^c}\right), \quad B = \left(\Delta\chi, \Delta D_\eta, \Delta D_\tau, \Delta\lambda_\eta^t, \Delta\lambda_\eta^c\right), \quad C = (\upsilon, \beta), \tag{2.34}$$

where A is intended as the Frechet derivative of the energy functional, the first variation $\delta\mathcal{E}$ of the energy functional in (2.30) and its increment $\Delta\mathcal{E}$ in (2.32) are represented as linear functional of the variation C and the increment B as follows,

$$\delta\mathcal{E} = A \cdot C, \qquad \Delta\mathcal{E} = A \cdot B, \tag{2.35}$$

so that the hemi-variational principle (2.33) can be formulated

$$A \cdot B \leq A \cdot (\upsilon, \beta) \qquad \forall \upsilon \in AV_t, \qquad \forall \beta \in \mathbb{R}^+ \times \mathbb{R}^+ \times \mathbb{R}^+ \times \mathbb{R}^+. \tag{2.36}$$

As remarked in [36], the inequality (2.33) states that the actual energy release rate is not smaller than any possible one. Thus, it constitutes a kind of principle of maximum energy release rate.

2.5. The consequence of the hemivariational principle

First of all, the reversibility of the admissible placement variation $\upsilon = \delta\chi \in AV_t$ implies

$$\mathcal{E}\left(\chi + \delta\chi, D_\eta, D_\tau, \lambda_\eta^t, \lambda_\eta^c\right) - \mathcal{E}\left(\chi, D_\eta, D_\tau, \lambda_\eta^t, \lambda_\eta^c\right) = \frac{\partial \mathcal{E}}{\partial \chi}\delta\chi = 0, \qquad \forall \upsilon = \delta\chi \in AV_t, \tag{2.37}$$

that correspond to standard strain gradient elasticity equations for fixed values of irreversible kinematic quantities $\left(D_\eta, D_\tau, \lambda_\eta^t, \lambda_\eta^c\right)$. Equation (2.37) is derived simply evaluating the inequality (2.36) both for $\delta\chi = \Delta\chi + \hat{\delta}\chi$ and $\beta = \left(\Delta D_\eta, \Delta D_\tau, \Delta\lambda_\eta^t, \Delta\lambda_\eta^c\right)$ and for $\delta\chi = \Delta\chi - \hat{\delta}\chi$ and $\beta = \left(\Delta D_\eta, \Delta D_\tau, \Delta\lambda_\eta^t, \Delta\lambda_\eta^c\right)$, where $\hat{\delta}\chi$ is another arbitrary variation that in (2.37) takes the same symbol $\delta\chi$ just for the sake of simplicity. Secondly, following [47], the variational inequality (2.36) implies the following KKT conditions on the 4 irreversible kinematic descriptors $\left(D_\eta, D_\tau, \lambda_\eta^t, \lambda_\eta^c\right)$

$$\left\{D_\eta - \tilde{D}_\eta(u_\eta, \lambda_\eta^t, \lambda_\eta^c)\right\}\Delta D_\eta = 0 \tag{2.38}$$

$$\left\{D_\tau - \tilde{D}_\tau(u_\tau)\right\}\Delta D_\tau = 0 \tag{2.39}$$

$$\left\{\lambda_\eta^t - \tilde{\lambda}_\eta^t(u_\eta, \lambda_\eta^c, D_\eta, D_\tau)\right\}\Delta\lambda_\eta^t = 0 \tag{2.40}$$

$$\left\{\lambda_\eta^c - \tilde{\lambda}_\eta^c(u_\eta, \lambda_\eta^t, D_\eta, D_\tau)\right\}\Delta\lambda_\eta^c = 0, \tag{2.41}$$

where the derivation of (2.38) is done simply evaluating the inequality (2.36) both for $\delta\chi = \Delta\chi$ and $\beta = \left(2\Delta D_\eta, \Delta D_\tau, \Delta\lambda_\eta^t, \Delta\lambda_\eta^c\right)$ and for $\delta\chi = \Delta\chi$ and $\beta = \left(0, \Delta D_\tau, \Delta\lambda_\eta^t, \Delta\lambda_\eta^c\right)$, the derivation of (2.39) is done simply evaluating the inequality (2.36) both for $\delta\chi = \Delta\chi$ and $\beta = \left(\Delta D_\eta, 2\Delta D_\tau, \Delta\lambda_\eta^t, \Delta\lambda_\eta^c\right)$ and for $\delta\chi = \Delta\chi$ and $\beta = \left(\Delta D_\eta, 0, \Delta\lambda_\eta^t, \Delta\lambda_\eta^c\right)$, the derivation of (2.40) is done simply evaluating the inequality (2.36) both for $\delta\chi = \Delta\chi$ and $\beta = \left(\Delta D_\eta, \Delta D_\tau, 2\Delta\lambda_\eta^t, \Delta\lambda_\eta^c\right)$ and for $\delta\chi = \Delta\chi$ and $\beta = \left(\Delta D_\eta, \Delta D_\tau, 0, \Delta\lambda_\eta^c\right)$ and the derivation of (2.41) is done simply evaluating the inequality (2.36) both for $\delta\chi = \Delta\chi$ and $\beta = \left(\Delta D_\eta, \Delta D_\tau, \Delta\lambda_\eta^t, 2\Delta\lambda_\eta^c\right)$ and for $\delta\chi = \Delta\chi$ and $\beta = \left(\Delta D_\eta, \Delta D_\tau, \Delta\lambda_\eta^t, 0\right)$. In (2.38)–(2.41) the auxiliary threshold functions $\tilde{D}_\eta(u_\eta, \lambda_\eta^t, \lambda_\eta^c)$, $\tilde{D}_\tau(u_\tau)$, $\tilde{\lambda}_\eta^t(u_\eta, \lambda_\eta^c, D_\eta, D_\tau)$ and $\tilde{\lambda}_\eta^c(u_\eta, \lambda_\eta^t, D_\eta, D_\tau)$ have been defined as follows,

$$\tilde{D}_\eta(u_\eta, \lambda_\eta^t, \lambda_\eta^c) = \begin{cases} 1 - \exp\left(-\frac{u_\eta - \lambda_\eta^t + \lambda_\eta^c}{B_\eta^t}\right), & u_\eta^{el} = u_\eta - \lambda_\eta^t + \lambda_\eta^c > 0, \\ \frac{2}{\pi}\arctan\left(-\frac{u_\eta - \lambda_\eta^t + \lambda_\eta^c}{B_\eta^c}\right), & u_\eta^{el} = u_\eta - \lambda_\eta^t + \lambda_\eta^c < 0, \end{cases} \tag{2.42}$$

$$\tilde{D}_\tau(u_\tau) = 1 - \exp\left(-\frac{|u_\tau|}{B_\tau}\right), \tag{2.43}$$

$$\tilde{\lambda}_\eta^t(u_\eta, \lambda_\eta^c, D_\eta, D_\tau) = \lambda_\eta^c - \frac{\sigma_\eta^t}{k_\eta\left(1 - D_\eta\right)} + u_\eta + \frac{k_\tau B_\tau}{k_\eta\left(1 - D_\eta\right)}\frac{\partial \widetilde{B}_\tau}{\partial u_\eta^{el}}\left[\int_0^{D_\tau}\left[\log\left(1 - x\right)\right]^2 dx\right], \tag{2.44}$$

$$\tilde{\lambda}^c_\eta(u_\eta, \lambda^t_\eta, D_\eta, D_\tau) = \lambda^t_\eta - \frac{\sigma^c_\eta}{k_\eta\left(1-D_\eta\right)} - u_\eta - \frac{k_\tau B_\tau}{k_\eta\left(1-D_\eta\right)}\frac{\partial \widetilde{B}_\tau}{\partial u^{el}_\eta}\left[\int_0^{D_\tau}\left[\log\left(1-x\right)\right]^2 dx\right]. \quad (2.45)$$

From Eqs (2.42) and (2.43) the meaning of B^t_η, B^c_η and B_τ as characteristic displacements for the activation of the damage phenomena is evident at least for the loading case. Besides, we observe from (2.44) and (2.45) that with no damage, the meaning of the scalars σ^t_η and σ^c_η as those characteristic forces that dictate the yielding conditions in tension and compression, is also explained. However, the presence of the normal damage D_η makes higher such effective characteristic displacement that, in the failure case (with $D_\eta \to 1$), becomes infinite.

3. Implementation of the model

In this Section, the implementation of the model previously presented is divided in the following 5 steps.

1) Null initial, i.e., at time $t = 0$, conditions is assumed on the displacement field for all the points of the body

$$u\left(\boldsymbol{X}, t=0\right) = \boldsymbol{\chi}\left(\boldsymbol{X}, t=0\right) - \boldsymbol{X} = 0, \quad \forall \boldsymbol{X} \in \mathcal{B} \quad (3.1)$$

and and the same for damage and plastic irreversible descriptors both for all the points of the body and for all the directions,

$$\begin{cases} D_\eta = \breve{D}_\eta\left(\hat{c}, \boldsymbol{X}, t=0\right) = 0, & D_\tau = \breve{D}_\tau\left(\hat{c}, \boldsymbol{X}, t=0\right) = 0 \\ \lambda^t_\eta = \breve{\lambda}^t_\eta\left(\hat{c}, \boldsymbol{X}, t=0\right) = 0, & \lambda^c_\eta = \breve{\lambda}^c_\eta\left(\hat{c}, \boldsymbol{X}, t=0\right) = 0 \end{cases}, \qquad \forall \hat{c} \in \mathcal{S}^1 \quad \forall \boldsymbol{X} \in \mathcal{B} \quad (3.2)$$

2) Initial isotropy is assumed, that means that non-damaged stiffnesses k^c_η, k^t_η and k_τ are assumed to be initially constant $\forall \hat{c} \in \mathcal{S}^1$ and $\forall \boldsymbol{X} \in \mathcal{B}$

$$k^c_\eta = \tilde{k}^c_\eta\left(\hat{c}, \boldsymbol{X}, t=0\right) = \frac{\bar{k}^c_\eta}{2\pi}, \quad k^t_\eta = \tilde{k}^t_\eta\left(\hat{c}, \boldsymbol{X}, t=0\right) = \frac{\bar{k}^t_\eta}{2\pi}, \quad k_\tau = \tilde{k}_\tau\left(\hat{c}, \boldsymbol{X}, t=0\right) = \frac{\bar{k}_\tau}{2\pi}, \quad (3.3)$$

where $\bar{k}^c_\eta$, $\bar{k}^t_\eta$ and $\bar{k}_\tau$ are the averaged non-damaged initial stiffnesses.

3) Numerical values of the parameters of the model are assumed and here are reported in Tables 1 and 2.

4) The elastic stiffness tensors ($\mathbb{C}, \mathbb{M}, \mathbb{D}$), as well as the pre-stress and pre hyperstress tensors ($\mathbb{P}, \mathbb{Q}$) are calculated according to Eqs (2.13)–(2.17) at time $t = 0$ with the initial input (3.1)–(3.3). These ingredients with proper boundary conditions are the input for a standard variational principle in (2.37), where the dissipation energy becomes simply an additive constant that does not influence the minimization process. Such a minimization can be performed analytically (as in the homogeneous cases of Section 4) or, more generally, with the use of a Finite Element Method (FEM). Thus, we obtain the displacement field at $i = 1$,

$$u\left(\boldsymbol{X}, t=T_i\right), \quad \forall \boldsymbol{X} \in \mathcal{B}. \quad (3.4)$$

5) With (3.4) we compute the new irreversible descriptors $\left(D_\eta, D_\tau, \lambda_\eta^t, \lambda_\eta^c\right)$ via the KKT conditions (2.38)–(2.41) at $i = 1$,

$$\begin{cases} D_\eta = \breve{D}_\eta\left(\hat{c}, \boldsymbol{X}, t = T_i\right), & D_\tau = \breve{D}_\tau\left(\hat{c}, \boldsymbol{X}, t = T_i\right) \\ \lambda_\eta^t = \breve{\lambda}_\eta^t\left(\hat{c}, \boldsymbol{X}, t = T_i\right), & \lambda_\eta^c = \breve{\lambda}_\eta^c\left(\hat{c}, \boldsymbol{X}, t = T_i\right) \end{cases}, \qquad \forall \hat{c} \in \mathcal{S}^1 \quad \forall \boldsymbol{X} \in \mathcal{B} \tag{3.5}$$

Thus, we iterate the points 4 and 5 for all those time sequence $T_i \in \{T_i\}_{i=0,\dots,M}$ with $T_i \in \mathbb{R}$ and $M \in \mathbb{N}$ of the researched time history defined at the beginning of Subsection 2.4.

Table 1. Constitutive parameters values employed for homogeneous extension/compression tests.

L[m]	A[m]	$\bar{k}_\eta^c[\frac{Kg}{s^2m^2}]$	$\bar{k}_\eta^t[\frac{Kg}{s^2m^2}]$	$\bar{k}_\tau[\frac{Kg}{s^2m^2}]$	B_η^t[m]	B_η^c[m]
0.01	0.1	$2\pi\, 14\, 10^{14}$	$10\bar{k}_\eta^c$	$2\pi\, 10^{13}$	10^{-8}	10^{-7}
$B_{\tau 0}$[m]	$\alpha_1[1]$	$\alpha_2[1]$	$\sigma_\eta^t[J/m^3]$	$\sigma_\eta^c[J/m^3]$	.	.
$5 \cdot 10^{-8}$	10	14	$8.385 \cdot 10^6$	$8.912 \cdot 10^7$	.	.

Table 2. Parameters for external boundary conditions employed for the investigated homogeneous tests.

α_c	α_t
$2\ 10^{-6} m/s$	$10^{-7} m/s$

4. Homogeneous response

Constitutive parameters are depicted in Table 1. Thus, from [12, 59] we have an equivalent initial Young modulus in compression E_c or in tension E_t and Poisson ratio in compression ν_c or in tension ν_t, that yields in compression

$$E_c = L^2 k_\eta^c \frac{k_\eta^c + 4k_\tau}{3k_\eta^c + 4k_\tau} = 299GPa, \quad \nu_c = \frac{k_\eta^c - 4k_\tau}{3k_\eta^c + 4k_\tau} = 0.32 \tag{4.1}$$

or in tension

$$E_t = L^2 k_\eta^t \frac{k_\eta^t + 4k_\tau}{3k_\eta^t + 4k_\tau} = 34.4GPa, \quad \nu_c = \frac{k_\eta^t - 4k_\tau}{3k_\eta^t + 4k_\tau} = 0.22. \tag{4.2}$$

Let us solve the problem in Figure 1. The imposed displacement is

$$\delta(t) = \alpha t \tag{4.3}$$

and, consequently, the displacement is trivially deduced in all the body,

$$u_1 = \frac{\alpha}{A} t X_1, \quad u_2 = 0, \qquad \forall X \in \mathcal{B}. \tag{4.4}$$

Thus, the strain and strain gradient are

$$G_{11} = \frac{\alpha}{A}t + \frac{1}{2}\left(\frac{\alpha}{A}t\right)^2, \quad G_{12} = G_{22} = 0, \quad \nabla G = 0, \tag{4.5}$$

and the relative displacements from (2.3) and (2.4) are

$$u_\eta = LG_{11}\cos\theta = L\left[\frac{\alpha}{A}t + \frac{1}{2}\left(\frac{\alpha}{A}t\right)^2\right]\cos\theta, \tag{4.6}$$

$$u_\tau^2 = 4L^2G_{11}G_{11}\left(\cos^4\theta - \cos^2\theta\right) = \left(L\left[\frac{\alpha}{A}t + \frac{1}{2}\left(\frac{\alpha}{A}t\right)^2\right]\sin 2\theta\right)^2, \tag{4.7}$$

where a standard parameterization of the unit vector $\hat{c}$ has been used in terms of an angle θ, i.e.,

$$\hat{c}_1 = \cos\theta, \quad \hat{c}_2 = \sin\theta. \tag{4.8}$$

The stress response is given in terms of the components of the stress tensors in (2.18),

$$S_{11} = \mathbb{P}_{11} + \mathbb{C}_{1111}G_{11}, \tag{4.9}$$

$$S_{22} = \mathbb{P}_{22} + \mathbb{C}_{2211}G_{11}, \tag{4.10}$$

$$S_{12} = \mathbb{P}_{12} + \mathbb{C}_{1211}G_{11}, \tag{4.11}$$

$$T = 0 \tag{4.12}$$

that implies

$$\begin{aligned} S_{11} &= -L\int_0^{2\pi}\left[k_\eta\left(1-D_\eta\right)\left(\lambda_\eta^t - \lambda_\eta^c\right)\cos^2\theta\right]d\theta \\ &+ G_{11}L^2\int_0^{2\pi}\left[k_\eta\left(1-D_\eta\right)\cos^4\theta + k_\tau\left(1-D_\tau\right)\left(4\cos^2\theta - 4\cos^4\theta\right)\right]d\theta, \end{aligned} \tag{4.13}$$

$$\begin{aligned} S_{22} &= -L\int_0^{2\pi}\left[k_\eta\left(1-D_\eta\right)\left(\lambda_\eta^t - \lambda_\eta^c\right)\sin^2\theta\right]d\theta \\ &+ G_{11}L^2\int_0^{2\pi}\left[k_\eta\left(1-D_\eta\right)\sin^2\theta\cos^2\theta - 4k_\tau\left(1-D_\tau\right)\cos^4\theta\right]d\theta, \end{aligned} \tag{4.14}$$

$$S_{12} = 0, \qquad T = 0. \tag{4.15}$$

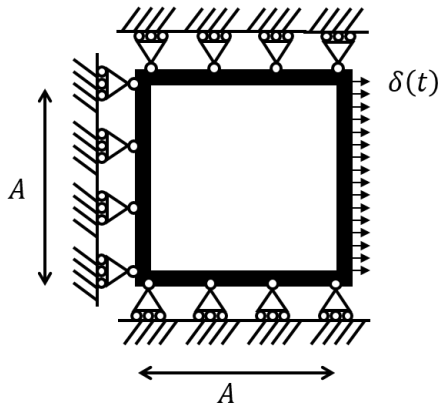

Figure 1. Schematic structure for the response to imposed displacement for tension ($\delta(t) > 0$) or compression ($\delta(t) < 0$) tests.

4.1. Strain tension control

In tension

$$\alpha = \alpha_t > 0 \tag{4.16}$$

the normal displacement $u_\eta \geq 0$ is positive in any direction (i.e., $\forall\theta \in [0, 2\pi]$) and therefore from (2.45) we have

$$\lambda_\eta^c = 0. \tag{4.17}$$

From (2.42) and (2.44) we have

$$\tilde{D}_\eta(u_\eta, \lambda_\eta^t, \lambda_\eta^c) = 1 - \exp\left(-\frac{u_\eta - \lambda_\eta^t}{B_\eta^t}\right), \quad \tilde{\lambda}_\eta^t(u_\eta, \lambda_\eta^c, D_\eta, D_\tau) = u_\eta - \frac{\sigma_\eta^t}{k_\eta\left(1 - D_\eta\right)}. \tag{4.18}$$

At the beginning of the time history (i.e., with $0 < u_\eta \ll L$ from (4.6)) we have from $(4.18)_2$ that $\tilde{\lambda}_\eta^t(u_\eta, \lambda_\eta^c, D_\eta, D_\tau) < 0$ that means an analytical solution for the accumulation in tension and for the normal damage,

$$\lambda_\eta^t = 0, \quad D_\eta = 1 - \exp\left(-\frac{u_\eta}{B_\eta^t}\right). \tag{4.19}$$

The solution (4.19) is valid only before the threshold condition (2.40) with (2.44)

$$\tilde{\lambda}_\eta^t(u_\eta, \lambda_\eta^c, D_\eta, D_\tau) = u_\eta - \frac{\sigma_\eta^t}{k_\eta\left(1 - D_\eta\right)} = 0 \tag{4.20}$$

is satisfied. Thus, by insertion of $(4.19)_2$ into (4.20) we have,

$$\left(1 - D_\eta\right) = \frac{\sigma_\eta^t}{k_\eta u_\eta} = \exp\left(-\frac{u_\eta}{B_\eta^t}\right). \tag{4.21}$$

The nonlinear algebraic equation (4.21) defines a Lambert function, does not have an analytical solution and can be solved only numerically or graphically, e.g., in Figure 2, from which it is clear, with the constitutive parameters that we have chosen in Table 1, that the condition (4.21) is satisfied for no values of the normal displacement u_η, that implies that $(4.19)_1$ is always valid in this investigated case and no plastic behavior takes place. Besides, a different choice of the normal damage characteristic displacement B_η^t would give a different result. From Figure 2 it is in fact also shown that by assigning a value of the normal damage characteristic displacement B_η^t equal to 20 times that assigned in Table 1, there exist a value for the normal displacement $u_\eta = \check{u}_\eta$ that satisfies (4.21),

$$\frac{\sigma_\eta^t}{k_\eta u_\eta} = \exp\left(-\frac{u_\eta}{B_\eta^t}\right), \quad \Rightarrow \quad u_\eta = \check{u}_\eta \tag{4.22}$$

that implies that $(4.19)_1$ is not valid and plasticity takes a role in this new investigated case. The new analytical solution comes from (4.18), from which we derive the nonlinear algebraic equation for normal damage

$$1 - D_\eta = \exp\left(-\frac{\sigma_\eta^t}{B_\eta^t k_\eta\left(1 - D_\eta\right)}\right), \quad \Rightarrow \quad D_\eta = \check{D}_\eta, \quad u_\eta > \check{u}_\eta \tag{4.23}$$

and for accumulation of tension

$$\lambda_\eta^t = u_\eta - \frac{\sigma_\eta^t}{k_\eta\left(1-\check{D}_\eta\right)}, \quad u_\eta > \check{u}_\eta \tag{4.24}$$

We observe from (4.23) that the normal damage $D_\eta = \check{D}_\eta$ at which the condition $u_\eta = \check{u}_\eta > 0$ holds is constant with respect to the normal displacement u_η and therefore with respect to time. This implies that the accumulation in tension in (4.24) evolves linearly with the normal displacement.

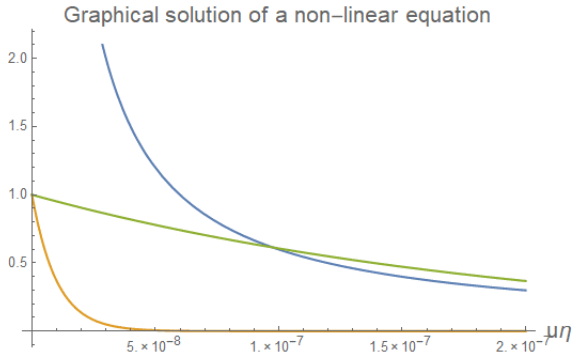

Figure 2. Numerical investigation of (4.21) with parameters assigned in Table 1 and with 20 times the value of normal damage characteristic displacement B_η^t. Blue curve is the left-hand side of (4.21), i.e., $\frac{\sigma_\eta^t}{k_\eta u_\eta}$. Orange line is the right-hand side of (4.21), i.e., $\exp\left(-\frac{u_\eta}{B_\eta^t}\right)$. Blue and orange lines do not intersect and therefore there is no solution $\check{u}$ of (4.22). Green line is the right-hand side of (4.21) with B_η^t being 20 times that represented in Table 1, i.e., $\exp\left(-\frac{u_\eta}{20B_\eta^t}\right)$. Blue and green lines do intersect and therefore there is a solution $\check{u}$ of (4.22) in this case.

The response is calculated by (4.13)–(4.15) and it is graphically represented in Figure 3. We observe (S_{11} in the left-hand side of Figure 3) that, after a first part where we have an increasing function of time, in a second part of the response the softening induced by damage is evident and a peak reaction is observed as well as a descending curve. A positive reaction is observed also in the orthogonal direction (S_{22} in the right-hand side of Figure 3). The behavior in the orthogonal direction is almost equivalent. However, a second hardening stage is observed because of a non trivial evolution of the equivalent (the response is not anymore isotropic) Poisson ratio.

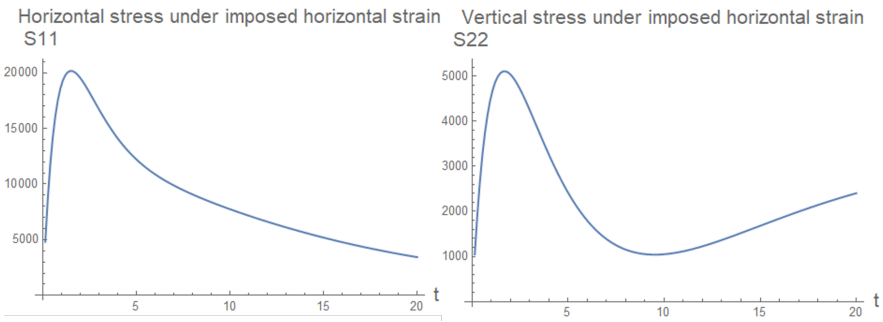

Figure 3. Stress response to imposed axial displacement in tension depicted in Figure 1.

The softening behavior is due the non homogeneous evolution of the damage variables with respect to the grain-pair orientation $\hat{c} \in \mathcal{S}^1$ or, equivalently, to the angle $\theta \in [0, 2\pi]$, as it is shown in Figure 4.

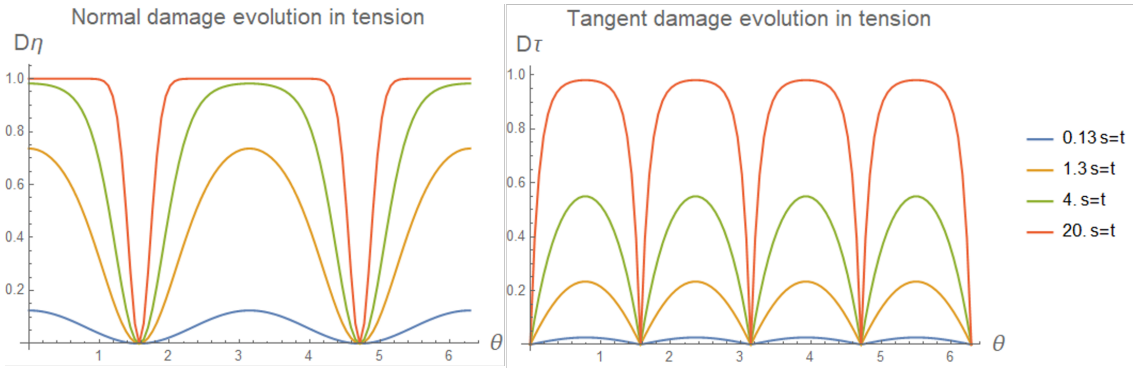

Figure 4. Evolution of normal and tangent damage for the case of axial displacement in tension imposed and depicted in Figure 1.

The anisotropic behavior is also explicated in the evolution of the ratio $\mathbb{C}_{2222}/\mathbb{C}_{1111}$ between the vertical and the horizontal stiffness in Figure 5.

In the left-hand side picture of Figure 4 normal damage evolution is shown and it is evident that the horizontal grain-pair orientation, i.e., around $\theta = k\pi$, with $k \in \mathbb{Z}$, are the most affected by the damage effect. In the right-hand side picture of Figure 4 tangential damage evolution is shown and it is evident that the oblique grain-pair orientation, i.e., around $\theta = \pi/4 + k\pi/2$, with $k \in \mathbb{Z}$, are the most affected by the damage effect. It is also observed that the velocity of the damage evolution is constitutively driven by the damage characteristic displacements B^t_η, B^c_η and B_τ. It is also worth to be noted from Figure 5 that the anisotropy between vertical and horizontal stiffness on the one hand in an elastic isotropic simulation should be maintained at 1 for the entire history of deformation. Here, on the other hand, it goes from 1 at $t = 0$ (i.e., initial isotropic behavior) to 60 at $t = 20s$ (i.e., we have anisotropic behavior induced by deformation).

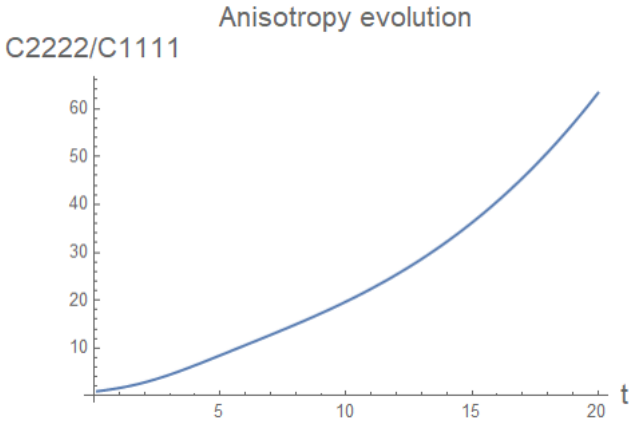

Figure 5. Evolution of the ratio $\mathbb{C}_{2222}/\mathbb{C}_{1111}$, that is the ratio between the vertical and the horizontal stiffness for the case of axial displacement in tension imposed depicted in Figure 1.

As it is shown in Figure 2 on the one hand no plastic behavior occurs in this case. On the other hand, increasing 20 times the normal damage characteristic displacement ($B^t_\eta \to 20B^t_\eta$), the response changes dramatically. In Figure 6 the stress response is shown in this second case and the softening behavior is very much attenuated.

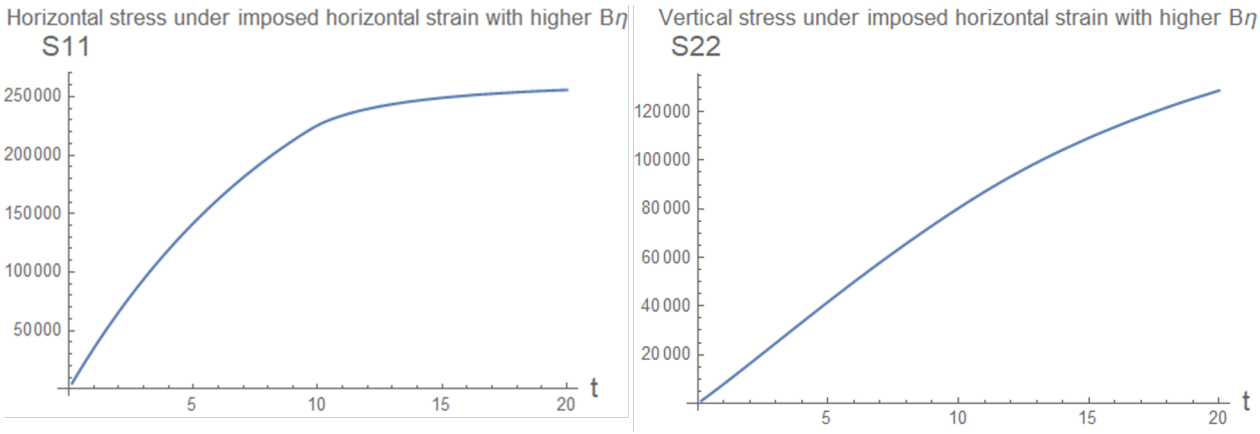

Figure 6. Stress response to imposed axial displacement in tension depicted in Figure 1 and higher normal damage characteristic displacement.

In Figure 7 normal and tangent damage evolution are also different. In fact, e.g., maximum normal damage is not any more equal to the admissible value $D_\eta \simeq 1$ but to the constant value $D_\eta = \check{D}_\eta \simeq 0.4$ that was analytically calculated in (4.23).

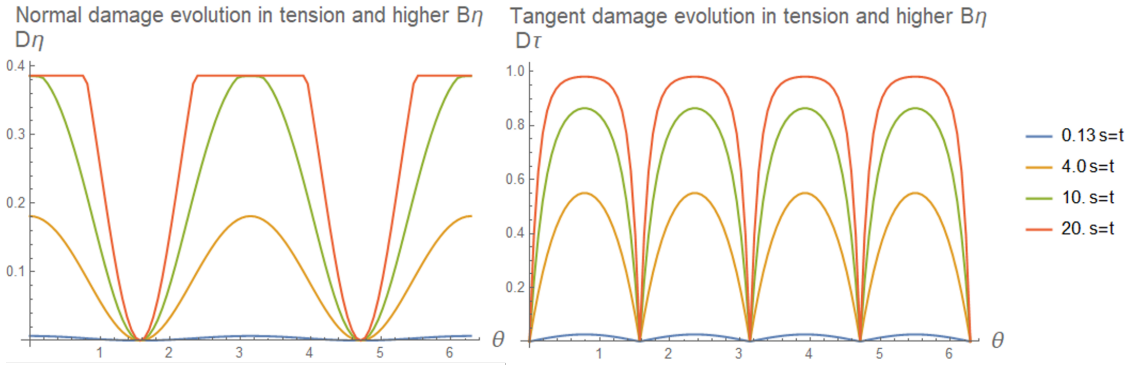

Figure 7. Evolution of normal and tangent damage for the case of axial displacement in tension imposed depicted in Figure 1 and higher normal damage characteristic displacement.

The non trivial plastic displacement evolution $u^{pl}_\eta = \lambda^t_\eta - \lambda^c_\eta$ is therefore shown in Figure 8. It is evident that the plastic displacement occurs only around the horizontal direction.

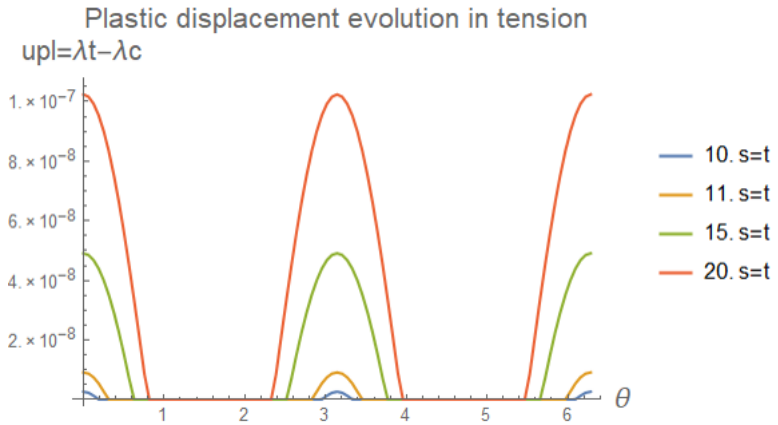

Figure 8. Evolution of plastic displacement $u_\eta^{pl} = \lambda_\eta^t - \lambda_\eta^c$ for the case of axial displacement in tension imposed depicted in Figure 1 and higher normal damage characteristic displacement.

4.2. Strain compression control

In compression

$$\alpha = -\alpha_c < 0. \tag{4.25}$$

the relative displacement $u_\eta \leq 0$ is negative in any direction (i.e., $\forall\theta \in [0, 2\pi]$) and therefore from (2.44) we have

$$\lambda_\eta^t = 0. \tag{4.26}$$

From (2.42) and (2.44) we have

$$\tilde{D}_\eta(u_\eta, \lambda_\eta^t, \lambda_\eta^c) = \frac{2}{\pi}\arctan\left(-\frac{u_\eta + \lambda_\eta^c}{B_\eta^c}\right), \quad \tilde{\lambda}_\eta^c(u_\eta, \lambda_\eta^c, D_\eta, D_\tau) = -u_\eta - \frac{\sigma_\eta^c}{k_\eta\left(1 - D_\eta\right)}. \tag{4.27}$$

At the beginning of the time history (i.e., with $0 \geq u_\eta \gg -L$ from (4.6)) we have from $(4.27)_2$ that $\tilde{\lambda}_\eta^c(u_\eta, \lambda_\eta^c, D_\eta, D_\tau) < 0$ that means an analytical solution for the accumulation in compression and for the normal damage as follows,

$$\lambda_\eta^c = 0, \quad D_\eta = \frac{2}{\pi}\arctan\left(-\frac{u_\eta}{B_\eta^c}\right). \tag{4.28}$$

The solution (4.28) is valid only before the threshold condition (2.41) with (2.45)

$$\tilde{\lambda}_\eta^c(u_\eta, \lambda_\eta^c, D_\eta, D_\tau) = -u_\eta - \frac{\sigma_\eta^c}{k_\eta\left(1 - D_\eta\right)} = 0 \tag{4.29}$$

is satisfied. Thus, by insertion of $(4.28)_2$ into (4.29) we have,

$$\left(1 - D_\eta\right) = \frac{-\sigma_\eta^c}{k_\eta u_\eta} = 1 - \frac{2}{\pi}\arctan\left(-\frac{u_\eta}{B_\eta^c}\right). \tag{4.30}$$

With the constitutive parameters that we have chosen in Table 1 this condition happens at $u_\eta = \bar{u}_\eta < 0$ and therefore we have (4.28) for $u_\eta < \bar{u}_\eta$

$$\lambda_\eta^c = -u_\eta - \frac{\sigma_\eta^c}{k_\eta\left(1 - D_\eta\right)}, \quad D_\eta = \frac{2}{\pi}\arctan\left(-\frac{u_\eta + \lambda_\eta^c}{B_\eta^c}\right). \tag{4.31}$$

By insertion of (4.31) into (4.30) we also obtain a nonlinear algebraic equation

$$D_\eta = \frac{2}{\pi}\arctan\left(\frac{\sigma_\eta^c}{k_\eta B_\eta^c\left(1 - D_\eta\right)}\right), \quad \Rightarrow \quad D_\eta = \bar{D}_\eta \tag{4.32}$$

the solution of which gives the normal damage $D_\eta = \bar{D}_\eta$ at which the condition $u_\eta = \bar{u}_\eta < 0$ holds and that is constant with respect to the normal displacement u_η and therefore with respect to time. This implies that the accumulation in compression evolves linearly with the normal displacement by insertion of (4.32) into $(4.31)_2$,

$$\lambda_\eta^c = -u_\eta - \frac{\sigma_\eta^c}{k_\eta\left(1 - \bar{D}_\eta\right)}, \quad u_\eta < \bar{u}_\eta < 0 \tag{4.33}$$

This response is calculated by (4.13)–(4.15) and it is graphically represented in Figure 9. We observe ($S_{11} < 0$ in the left-hand side of Figure 9) that, after a first part where we have an decreasing function of time, in a second part of the response the softening induced by damage is evident and a peak reaction is observed as well as a slightly increasing curve. A negative reaction is observed also in the orthogonal direction ($S_{22} < 0$ in the right-hand side of Figure 9). The behavior in the orthogonal direction is almost equivalent except for the slightly increasing part again because of a non trivial evolution of the equivalent (the response is not anymore isotropic) Poisson ratio.

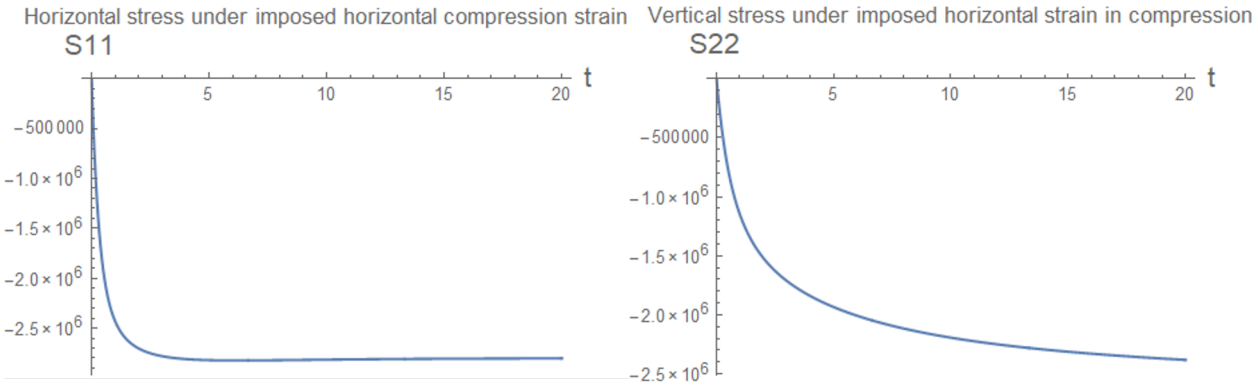

Figure 9. Stress response to imposed axial displacement in compression depicted in Figure 1.

The softening behavior is due the non homogeneous evolution of the damage variables with respect to the grain-pair orientation $\hat{c} \in \mathcal{S}^1$ or, equivalently, to the angle $\theta \in [0, 2\pi]$, as it is shown in Figure 10.

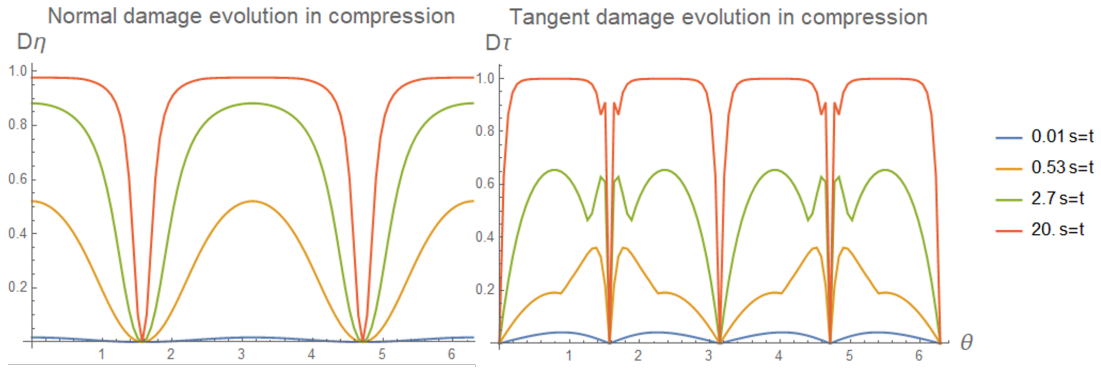

Figure 10. Evolution of normal and tangent damage for the case of axial displacement in compression imposed depicted in Figure 1.

The anisotropic behavior is also explicated in the evolution of the ratio $\mathbb{C}_{2222}/\mathbb{C}_{1111}$ between the vertical and the horizontal stiffness in Figure 11.

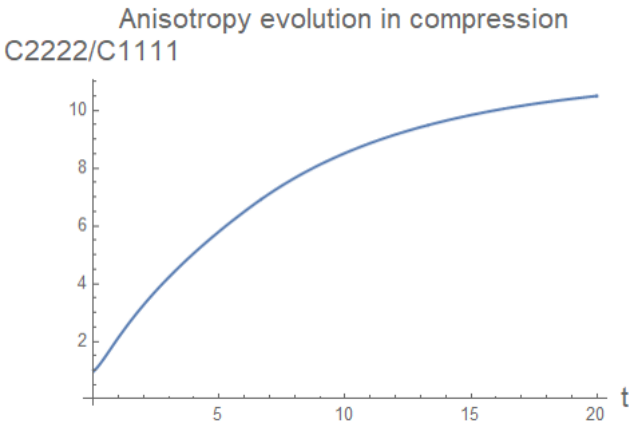

Figure 11. Evolution of the ratio $\mathbb{C}_{2222}/\mathbb{C}_{1111}$, that is the ratio between the vertical and the horizontal stiffness for the case of axial displacement in compression imposed depicted in Figure 1.

In the left-hand side picture of Figure 10 normal damage evolution is shown and it is evident that the horizontal grain-pair orientation, i.e., around $\theta = k\pi$, with $k \in \mathbb{Z}$, are the most affected by the damage effect. In the right-hand side picture of Figure 10 tangential damage evolution is shown and it is evident that the oblique grain-pair orientation, i.e., around $\theta = \pi/4 + k\pi/2$, with $k \in \mathbb{Z}$, are the most affected by the damage effect. This behavior is nevertheless obscured by the non constant dependence of the damage tangential characteristic displacement B_τ with respect to the normal displacement in compression that was made explicit in (2.23). We have that the higher is the compression the lower is the damage velocity evolution. Thus, the orientation that are more in compression, i.e., $\theta = k\pi$, with $k \in \mathbb{Z}$, have lower damage velocity evolution with respect to the orientation that are less in compression, i.e., $\theta = \pi/2 + k\pi$, with $k \in \mathbb{Z}$, where damage have new peaks.

It is also worth to be noted from Figure 11 that the anisotropy between vertical and horizontal stiffness on the one hand in an elastic isotropic simulation should be maintained at 1 for the entire

history of deformation. Here, on the other hand, it goes from 1 at $t = 0$ (i.e., initial isotropic behavior) to 13 at $t = 20s$ (i.e., anisotropic behavior induced by deformation).

The non trivial plastic displacement evolution $u_\eta^{pl} = \lambda_\eta^t - \lambda_\eta^c$ is therefore shown in Figure 12. It is evident that the plastic displacement occurs only around the horizontal direction.

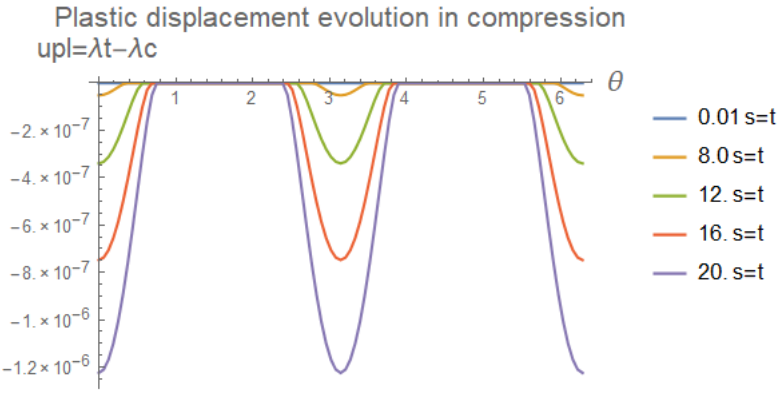

Figure 12. Evolution of plastic displacement for the case of axial displacement in compression imposed depicted in Figure 1 and higher normal damage characteristic displacement.

5. Conclusions

This paper recaps and updates a recently developed continuum model for granular materials in order to handle with those important dissipative phenomena as damage and plasticity. The novelty of such a recap is original. The reason is that here for the first time the dissipation energy and the variational inequality are defined directly integrated over the orientation space. This makes the Euler Lagrange equations related to the displacement field (i.e., the elastic Partial Differential Equations PDEs and Boundary Conditions BCs) already integrated over that space. The advantage is that we derive directly the equations that we use for the numerical integration and we do not need to make an artificial integration after their derivation. Its application to an analytical homogeneous case is considered. Plasticity is given by two separate kinematic descriptors (i.e., the accumulation in tension and the accumulation in compression), that are the two plastic multipliers, for every position, time, and grain pair orientation. A hemi-variational principle was adopted to derive the governing equations, from which we obtain Karush-Kuhn-Tucker (KKT)-kind conditions that specify the progression of damage and plasticity relating to each pair of grains interaction. For the case of homogeneous deformation, an analytical solution for the displacement field is assumed and damage and plastic evolution have been derived. It is worth to remark that for non homogeneous deformation, the computation of non homogeneous strain can be reached, e.g., with a Finite Element method according to the scheme developed in [47, 59], where the presence of strain gradient terms in the PDEs related to the elastic evolution guarantees the overlook of the problem of the mesh-dependence results. Different loading patterns are experienced by different grain-pairs that are oriented in different directions, resulting in complex anisotropic behavior due to damage and plastic evolution. Competition between damage and plasticity dissipative phenomena is demonstrated in these simulations. We show that, for specific parameters, the evolution of plasticity may stop the growth of

damage and vice versa. Besides, the presence of newly conceived constitutive parameters that are present in the dissipation energy functional, imposes a fundamental outlook related to their identification. In the presented model we have the inclusion of simple local plastic interactions that contribute to a complex plastic response of the material as a whole. Finally, no additional assumptions, out of the form of the dissipation energy and such as flow rules, are required to describe the plastic behavior and it is worth to point out that the plastic strain is compatible with the existence of a placement function.

Acknowledgments

This project has received funding from the European Union's Horizon 2020 research and innovation programme under the Marie Skłodowska-Curie grant agreement No 899546.

Conflict of interest

All authors declare no conflicts of interest in this paper

References

1. B. E. Abali, W. H. Müller, F. dell'Isola, Theory and computation of higher gradient elasticity theories based on action principles, *Arch. Appl. Mech.*, **87** (2017), 1495–1510. http://dx.doi.org/10.1007/s00419-017-1266-5

2. E. C. Aifantis, Pattern formation in plasticity, *Int. J. Eng. Sci.*, **33** (1995), 2161–2178. http://dx.doi.org/10.1016/0020-7225(95)00086-D

3. E. C. Aifantis, On the microstructural origin of certain inelastic models, *J. Eng. Mater. Technol.*, **106** (1984), 326–330. http://dx.doi.org/10.1115/1.3225725

4. E. C. Aifantis, The physics of plastic deformation, *Int. J. Plasticity*, **3** (1987), 211–247. http://dx.doi.org/10.1016/0749-6419(87)90021-0

5. J.-J. Alibert, A. Della Corte, I. Giorgio, A. Battista, Extensional Elastica in large deformation as\Gamma-limit of a discrete 1D mechanical system, *Z. Angew. Math. Phys.*, **68** (2017), 42. http://dx.doi.org/10.1007/s00033-017-0785-9

6. J. Altenbach, H. Altenbach, V. A. Eremeyev, On generalized cosserat-type theories of plates and shells: a short review and bibliography, *Arch. Appl. Mech.*, **80** (2010), 73–92. http://dx.doi.org/10.1007/s00419-009-0365-3

7. M. Ambati, T. Gerasimov, L. De Lorenzis, Phase-field modeling of ductile fracture, *Comput. Mech.*, **55** (2015), 1017–1040. http://dx.doi.org/10.1007/s00466-015-1151-4

8. M. Ambati, T. Gerasimov, L. De Lorenzis. A review on phase-field models of brittle fracture and a new fast hybrid formulation, *Comput. Mech.*, **55** (2015), 383–405. http://dx.doi.org/10.1007/s00466-014-1109-y

9. L. Ambrosio, A. Lemenant, G. Royer-Carfagni, A variational model for plastic slip and its regularization via Γ-convergence, *J. Elast.*, **110** (2013), 201–235. http://dx.doi.org/10.1007/s10659-012-9390-5

10. H. Amor, J.-J. Marigo, C. Maurini, Regularized formulation of the variational brittle fracture with unilateral contact: numerical experiments, *J. Mech. Phys. Solids*, **57** (2009), 1209–1229. http://dx.doi.org/10.1016/j.jmps.2009.04.011

11. N. Auffray, F. dell'Isola, V. Eremeyev, A. Madeo, G. Rosi, Analytical continuum mechanics à la Hamilton-Piola least action principle for second gradient continua and capillary fluids, *Math. Mech. Solids*, **20** (2015), 375–417. http://dx.doi.org/10.1177/1081286513497616

12. E. Barchiesi, A. Misra, L. Placidi, E. Turco, Granular micromechanics-based identification of isotropic strain gradient parameters for elastic geometrically nonlinear deformations, *Zeitschrift für Angewandte Mathematik und Mechanik*, **101** (2021), e202100059. http://dx.doi.org/10.1002/zamm.202100059

13. B. Bourdin, G. Francfort, J.-J. Marigo, Numerical experiments in revisited brittle fracture, *J. Mech. Phys. Solids*, **48** (2000), 797–826. http://dx.doi.org/10.1016/S0022-5096(99)00028-9

14. B. Bourdin, G. Francfort, J.-J. Marigo, The variational approach to fracture, *J. Eeast.*, **91** (2008), 5–148. http://dx.doi.org/10.1007/s10659-007-9107-3

15. L. Contrafatto, M. Cuomo, L. Greco, Meso-scale simulation of concrete multiaxial behaviour, *Eur. J. Environ. Civ. Eng.*, **21** (2017), 896–911. http://dx.doi.org/10.1080/19648189.2016.1182085

16. M. Cuomo, L. Contrafatto, L. Greco, A variational model based on isogeometric interpolation for the analysis of cracked bodies, *Int. J. Eng. Sci.*, **80** (2014), 173–188. http://dx.doi.org/10.1016/j.ijengsci.2014.02.017

17. M. Cuomo, A. Nicolosi, A poroplastic model for hygro-chemo-mechanical damage of concrete, *Computational modelling of concrete structures Conference*, Mayrhofen, Austria, 2006, 533–542.

18. F. D'Annibale, G. Rosi, A. Luongo, Linear stability of piezoelectric-controlled discrete mechanical systems under nonconservative positional forces, *Meccanica*, **50** (2015), 825–839. http://dx.doi.org/10.1007/s11012-014-0037-4

19. F. dell'Isola, A. D. Corte, I. Giorgio, Higher-gradient continua: The legacy of Piola, Mindlin, Sedov and Toupin and some future research perspectives, *Math. Mech. Solids*, **22** (2017), 852–872. http://dx.doi.org/10.1177/1081286515616034

20. F. dell'Isola, L. Placidi, Variational principles are a powerful tool also for formulating field theories, In: *Variational models and methods in solid and fluid mechanics*, Vienna: Springer, 2011, 1–15. http://dx.doi.org/10.1007/978-3-7091-0983-0_1

21. F. dell'Isola, M. Guarascio, K. Hutter, A variational approach for the deformation of a saturated porous solid. A second-gradient theory extending Terzaghi's effective stress principle, *Arch. Appl. Mech.*, **70** (2000), 323–337. http://dx.doi.org/10.1007/s004199900020

22. F. Freddi, G. Royer-Carfagni, Plastic flow as an energy minimization problem. Numerical experiments, *J. Elast.*, **116** (2014), 53–74. http://dx.doi.org/10.1007/s10659-013-9457-y

23. F. Freddi, G. Royer-Carfagni, Phase-field slip-line theory of plasticity, *J. Mech. Phys. Solids*, **94** (2016), 257–272. http://dx.doi.org/10.1016/j.jmps.2016.04.024

24. M. Froli, G. Royer-Carfagni, A mechanical model for the elastic–plastic behavior of metallic bars, *Int. J. Solids Struct.*, **37** (2000), 3901–3918. http://dx.doi.org/10.1016/S0020-7683(99)00069-4

25. I. Giorgio, Numerical identification procedure between a micro-Cauchy model and a macro-second gradient model for planar pantographic structures, *Z. Angew. Math. Phys.*, **67** (2016), 95. http://dx.doi.org/10.1007/s00033-016-0692-5

26. I. Giorgio, Lattice shells composed of two families of curved Kirchhoff rods: an archetypal example, topology optimization of a cycloidal metamaterial, *Continuum Mech. Thermodyn.*, **33** (2021), 1068–1082. http://dx.doi.org/10.1007/s00161-020-00955-4

27. I. Giorgio, A. Ciallella, D. Scerrato, A study about the impact of the topological arrangement of fibers on fiber-reinforced composites: some guidelines aiming at the development of new ultra-stiff and ultra-soft metamaterials, *Int. J. Solids Struct.*, **203** (2020), 73–83. http://dx.doi.org/10.1016/j.ijsolstr.2020.07.016

28. I. Giorgio, A. Culla, D. Del Vescovo, Multimode vibration control using several piezoelectric transducers shunted with a multiterminal network, *Arch. Appl. Mech.*, **79** (2009), 859. http://dx.doi.org/10.1007/s00419-008-0258-x

29. I. Giorgio, M. Spagnuolo, U. Andreaus, D. Scerrato, A. M. Bersani, In-depth gaze at the astonishing mechanical behavior of bone: A review for designing bio-inspired hierarchical metamaterials, *Math. Mech. Solids*, **26** (2020), 1074–1103. http://dx.doi.org/10.1177/1081286520978516

30. L. Greco, An iso-parametric G1-conforming finite element for the nonlinear analysis of Kirchhoff rod. Part I: the 2D case, *Continuum Mech. Thermodyn.*, **32** (2020), 1473–1496. http://dx.doi.org/10.1007/s00161-020-00861-9

31. P. Harrison, D. Anderson, M. F. Alvarez, E. Bali, Y. Mateos, Measuring and modelling the in-plane bending stiffness and wrinkling behaviour of engineering fabrics, *EUROMECH Colloquium 569: Multiscale Modeling of Fibrous and Textile Materials*, Chatenay-Malabry, France, 5–7 April 2016.

32. C. J. Larsen, A new variational principle for cohesive fracture and elastoplasticity, *Mech. Res. Commun.*, **58** (2014), 133–138. http://dx.doi.org/10.1016/j.mechrescom.2013.10.025

33. T. Y. Li, J.-J. Marigo, D. Guilbaud, S. Potapov, Variational approach to dynamic brittle fracture via gradient damage models, *Applied Mechanics and Materials*, **784** (2015), 334–341. http://dx.doi.org/10.4028/www.scientific.net/AMM.784.334

34. M. Malikan, V. A. Eremeyev, H. M. Sedighi, Buckling analysis of a non-concentric double-walled carbon nanotube, *Acta Mech.*, **231** (2020), 5007–5020. http://dx.doi.org/10.1007/s00707-020-02784-7

35. J.-J. Marigo, C. Maurini, K. Pham, An overview of the modelling of fracture by gradient damage models, *Meccanica*, **51** (2016), 3107–3128. http://dx.doi.org/10.1007/s11012-016-0538-4

36. J.-J. Marigo, Constitutive relations in plasticity, damage and fracture mechanics based on a work property, *Nucl. Eng. Des.*, **114** (1989), 249–272. http://dx.doi.org/10.1016/0029-5493(89)90105-2

37. C. Miehe, M. Hofacker, F. Welschinger, A phase field model for rate-independent crack propagation: Robust algorithmic implementation based on operator splits, *Comput. Method. Appl. Mech. Eng.*, **199** (2010), 2765–2778. http://dx.doi.org/10.1016/j.cma.2010.04.011

38. A. Misra, Effect of asperity damage on shear behavior of single fracture, *Eng. Fract. Mech.*, **69** (2002), 1997–2014. http://dx.doi.org/10.1016/S0013-7944(02)00073-5

39. A. Misra, P. Poorsolhjouy, Granular micromechanics model for damage and plasticity of cementitious materials based upon thermomechanics, *Math. Mech. Solids*, **25** (2020), 1778–1803. http://dx.doi.org/10.1177/1081286515576821

40. A. Misra, V. Singh, Thermomechanics-based nonlinear rate-dependent coupled damage-plasticity granular micromechanics model, *Continuum Mech. Thermodyn.*, **27** (2015), 787–817. http://dx.doi.org/10.1007/s00161-014-0360-y

41. A. Misra, L. Placidi, F. dell'Isola, E. Barchiesi, Identification of a geometrically nonlinear micromorphic continuum via granular micromechanics, *Z. Angew. Math. Phys.*, **72** (2021), 157. http://dx.doi.org/10.1007/s00033-021-01587-7

42. K. Naumenko, V. A. Eremeyev, A layer-wise theory of shallow shells with thin soft core for laminated glass and photovoltaic applications, *Compos. Struct.*, **178** (2017), 434–446. http://dx.doi.org/10.1016/j.compstruct.2017.07.007

43. L. Placidi, A variational approach for a nonlinear 1-dimensional second gradient continuum damage model, *Continuum Mech. Thermodyn.*, **27** (2015), 623–638. http://dx.doi.org/10.1007/s00161-014-0338-9

44. L. Placidi, A variational approach for a nonlinear one-dimensional damage-elasto-plastic second-gradient continuum model, *Continuum Mech. Thermodyn.*, **28** (2016), 119–137. http://dx.doi.org/10.1007/s00161-014-0405-2

45. L. Placidi, E. Barchiesi, Energy approach to brittle fracture in strain-gradient modelling, *Proc. R. Soc. A*, **474** (2018), 20170878. http://dx.doi.org/10.1098/rspa.2017.0878

46. L. Placidi, E. Barchiesi, A. Misra, A strain gradient variational approach to damage: a comparison with damage gradient models and numerical results, *Math. Mech. Complex Syst.*, **6** (2018), 77–100. http://dx.doi.org/10.2140/memocs.2018.6.77

47. L. Placidi, E. Barchiesi, A. Misra, D. Timofeev, Micromechanics-based elasto-plastic–damage energy formulation for strain gradient solids with granular microstructure, *Continuum Mech. Thermodyn.*, **33** (2021), 2213–2241. http://dx.doi.org/10.1007/s00161-021-01023-1

48. P. Poorsolhjouy, A. Misra, Effect of intermediate principal stress and loading-path on failure of cementitious materials using granular micromechanics, *Int. J. Solids Struct.*, **108** (2017), 139–152. http://dx.doi.org/10.1016/j.ijsolstr.2016.12.005

49. B. Reddy, The role of dissipation and defect energy in variational formulations of problems in strain-gradient plasticity. Part 1: polycrystalline plasticity, *Continuum Mech. Thermodyn.*, **23** (2011), 527–549. http://dx.doi.org/10.1007/s00161-011-0194-9

50. B. Reddy, The role of dissipation and defect energy in variational formulations of problems in strain-gradient plasticity. Part 2: Single-crystal plasticity, *Continuum Mech. Thermodyn.*, **23** (2011), 551. http://dx.doi.org/10.1007/s00161-011-0195-8

51. J. C. Reiher, I. Giorgio, A. Bertram, Finite-element analysis of polyhedra under point and line forces in second-strain gradient elasticity, *J. Eng. Mech.*, **143** (2017), 04016112. http://dx.doi.org/10.1061/(ASCE)EM.1943-7889.0001184

52. D. Scerrato, I. Giorgio, A. Della Corte, A. Madeo, N. Dowling, F. Darve, Towards the design of an enriched concrete with enhanced dissipation performances, *Cement Concrete Res.*, **84** (2016), 48–61. http://dx.doi.org/10.1016/j.cemconres.2016.03.002

53. D. Scerrato, I. Giorgio, A. Della Corte, A. Madeo, A. Limam, A micro-structural model for dissipation phenomena in the concrete, *Int. J. Numer. Anal. Meth. Geomech.*, **39** (2015), 2037–2052. http://dx.doi.org/10.1002/nag.2394

54. D. Scerrato, I. Giorgio, A. Madeo, A. Limam, F. Darve, A simple non-linear model for internal friction in modified concrete, *Int. J. Eng. Sci.*, **80** (2014), 136–152. http://dx.doi.org/10.1016/j.ijengsci.2014.02.021

55. P. Sicsic, J.-J. Marigo, From gradient damage laws to Griffith's theory of crack propagation, *J. Elast.*, **113** (2013), 55–74. http://dx.doi.org/10.1007/s10659-012-9410-5

56. M. Spagnuolo, U. Andreaus, A targeted review on large deformations of planar elastic beams: extensibility, distributed loads, buckling and post-buckling, *Math. Mech. Solids*, **24** (2019), 258–280. http://dx.doi.org/10.1177/1081286517737000

57. M. Spagnuolo, A. M. Cazzani, Contact interactions in complex fibrous metamaterials, *Continuum Mech. Thermodyn.*, **33** (2021), 1873–1889. http://dx.doi.org/10.1007/s00161-021-01018-y

58. M. Spagnuolo, M. E. Yildizdag, X. Pinelli, A. Cazzani, F. Hild, Out-of-plane deformation reduction via inelastic hinges in fibrous metamaterials and simplified damage approach, *Math. Mech. Solids*, 2021, in press. http://dx.doi.org/10.1177/10812865211052670

59. D. Timofeev, E. Barchiesi, A. Misra, L. Placidi, Hemivariational continuum approach for granular solids with damage-induced anisotropy evolution, *Math. Mech. Solids*, **26** (2021), 738–770. http://dx.doi.org/10.1177/1081286520968149

60. E. Turco, M. Golaszewski, A. Cazzani, N. L. Rizzi, Large deformations induced in planar pantographic sheets by loads applied on fibers: experimental validation of a discrete Lagrangian model, *Mech. Res. Commun.*, **76** (2016), 51–56. http://dx.doi.org/10.1016/j.mechrescom.2016.07.001

61. E. Turco, M. Golaszewski, I. Giorgio, F. D'Annibale, Pantographic lattices with non-orthogonal fibres: Experiments and their numerical simulations, *Compos. Part B: Eng.*, **118** (2017), 1–14. http://dx.doi.org/10.1016/j.compositesb.2017.02.039

62. Y. Yang, A. Misra, Micromechanics based second gradient continuum theory for shear band modeling in cohesive granular materials following damage elasticity, *Int. J. Solids Struct.*, **49** (2012), 2500–2514. http://dx.doi.org/10.1016/j.ijsolstr.2012.05.024